Backbone Dynamics of the *Bacillus subtilis* Glucose Permease IIA Domain Determined from ^{15}N NMR Relaxation Measurements†

Martin J. Stone,‡ Wayne J. Fairbrother,‡,∥ Arthur G. Palmer, III,‡,⊥ Jonathan Reizer,§ Milton H. Saier, Jr.,§ and Peter E. Wright*,‡

Department of Molecular Biology, The Scripps Research Institute, La Jolla, California 92037, and Department of Biology, University of California at San Diego, La Jolla, California 92093-0116

Received December 28, 1991

ABSTRACT: The backbone dynamics of the uniformly ^{15}N-labeled IIA domain of the glucose permease of *Bacillus subtilis* have been characterized using inverse-detected two-dimensional ^{1}H–^{15}N NMR spectroscopy. Longitudinal (T_1) and transverse (T_2) ^{15}N relaxation time constants and steady-state {^{1}H}–^{15}N NOEs were measured, at a spectrometer proton frequency of 500 MHz, for 137 (91%) of the 151 protonated backbone nitrogens. These data were analyzed by using a model-free dynamics formalism to determine the generalized order parameter (S^2), the effective correlation time for internal motions (τ_e), and ^{15}N exchange broadening contributions (R_{ex}) for each residue, as well as the overall molecular rotational correlation time (τ_m). The T_1 and T_2 values for most residues were in the ranges 0.45–0.55 and 0.11–0.15 s, respectively; however, a small number of residues exhibited significantly slower relaxation. Similarly, {^{1}H}–^{15}N NOE values for most residues were in the range 0.72–0.80, but a few residues had much smaller positive NOEs and some exhibited negative NOEs. The molecular rotational correlation time was 6.24 ± 0.01 ns; most residues had order parameters in the range 0.75–0.90 and τ_e values of less than ca. 25 ps. Residues found to be more mobile than the average were concentrated in three areas: the N-terminal residues (1–13), which were observed to be highly disordered; the loop from P25 to D41, the apex of which is situated adjacent to the active site and may have a role in binding to other proteins; and the region from A146 to S149. All mobile residues occurred in regions close to termini, in loops, or in irregular secondary structure.

Intramolecular motions of proteins, with characteristic time scales ranging from picoseconds to seconds (or longer), are important for enzyme catalysis, binding specificity, and regulatory control (Williams, 1979, 1989; Gurd & Rothgeb, 1979; Welch et al., 1982; Karplus & McCammon, 1983; Bennett & Huber, 1983; Ringe & Petsko, 1985). NMR[1] spectroscopy is uniquely suited to characterizing such internal motions; techniques available include measurements of relaxation rates (London, 1980; Nirmala & Wagner, 1988, 1989; Kay et al., 1989; Clore et al., 1990a; Palmer et al., 1991a), line-shape analyses (Nageswara Rao, 1989), magnetization transfer experiments (Alger & Shulman, 1984; Led et al., 1989), and amide isotope exchange measurements (Wagner, 1983; Englander & Kallenbach, 1983; Roder, 1989).

The measurement of ^{15}N and ^{13}C relaxation rates provides information about the internal dynamics of proteins on time scales faster than the rotational correlation time. The primary mechanism of relaxation for these nuclei is the dipolar interaction with the directly bound protons; chemical shift anisotropy (CSA) provides a secondary relaxation mechanism at high magnetic field strengths (Abragam, 1961; London, 1980). Recently, a number of reports have appeared in which ^{1}H-detected two-dimensional heteronuclear NMR experiments have been used to characterize ^{15}N or ^{13}C relaxation in proteins (Nirmala & Wagner, 1988; Kay et al., 1989; Clore et al., 1990a; Palmer et al., 1991a). Generally, the experimental results have been analyzed using the model-free formalism of Lipari and Szabo (1982a,b), in which the motions are described by the overall rotational correlation time, τ_m, a generalized order parameter, S^2, and an effective internal correlation time, τ_e. In particular cases, extensions to this formalism may be warranted (Clore et al., 1990a,b; Fedotov & Kivayeva, 1987; Zang et al., 1990).

Bacterial phosphoenolpyruvate/sugar phosphotransferase systems (PTS) are responsible for the concomitant translocation and phosphorylation of specific sugar substrates; additionally, the PTS regulates the uptake of other sugars by transcriptional and posttranscriptional mechanisms [for recent reviews, see Reizer et al. (1988), Saier (1989), and Meadow et al. (1990)]. The central regulatory protein of the PTS is the glucose-specific enzyme IIA (IIA^{Glc}, formerly referred to as enzyme III^{Glc} or factor III^{Glc}); regulation is effected by phosphorylation of a histidine residue. Transcriptional regulation of target operons by the PTS involves both catabolite repression and inducer exclusion (Magasanik, 1970). Cata-

† This work was supported by grants from the National Institutes of Health: GM-36643 (P.E.W.), RI-21702 (M.H.S.), and RI-14176 (M.H.S.). W.J.F. was supported by a Damon Runyon–Walter Winchell Cancer Research Fund Fellowship, DRG-1059. A.G.P. was supported by a National Science Foundation Postdoctoral Fellowship in Chemistry, under Grant CHE-8907510, awarded in 1989.

* To whom correspondence should be addressed.

‡ The Scripps Research Institute.

∥ Present address: Genentech Inc., 460 Point San Bruno Blvd., South San Francisco, CA 94080.

⊥ Present address: Department of Biochemistry and Biophysics, College of Physicians and Surgeons, Columbia University, 630 W. 168th St., New York, NY 10032.

§ University of California, San Diego.

[1] Abbreviations: IIA^{Glc}, *Bacillus subtilis* glucose permease IIA domain; NMR, nuclear magnetic resonance; T_1, longitudinal relaxation time constant; T_2, transverse relaxation time constant, $T_{1\rho}$, longitudinal relaxation time constant in the rotating frame; $T_{2\rho}$, transverse relaxation time constant in the rotating frame; NOE, nuclear Overhauser effect; NOESY, nuclear Overhauser effect spectroscopy; CSA, chemical shift anisotropy; PTS, phosphoenolpyruvate/sugar phosphotransferase system; 2D, two dimensional; CPMG, Carr–Purcell–Meiboom–Gill; FID, free induction decay; rms, root mean square; INEPT, insensitive nuclei enhanced by polarization transfer.

0006-2960/92/0431-4394$03.00/0

bolite repression is mediated by interactions between adenylate cyclase and phosphorylated IIA^{Glc}, which acts as an allosteric activator. Inducer exclusion involves direct allosteric inhibition, by unphosphorylated IIA^{Glc}, of target permeases and catabolic enzymes required to produce endogenous inducers of non-PTS operons. The activities of lactose permease and glycerol kinase are inhibited by direct binding of IIA^{Glc} (Osumi & Saier, 1982; Nelson et al., 1983; Saier et al., 1983; Postma et al., 1984; Novotny et al., 1985; de Boer et al., 1986). In addition to regulatory interactions, IIA^{Glc} interacts with both soluble (HPr) and membrane-bound (IIB^{Glc}) PTS proteins.

The glucose permease of *Bacillus subtilis* consists of the membrane-bound IICB domain covalently linked to a C-terminal IIA domain via a flexible Q-linker (Wootton & Drummond, 1989). The 162-residue IIA^{Glc} domain of *B. subtilis* has recently been overexpressed in *Escherichia coli* and assumes both the functional and regulatory roles of the soluble *E. coli* IIA^{Glc} protein when expressed in *crr* mutants, which are defective for the gene encoding IIA^{Glc} (Sutrina et al., 1990; Dean et al., 1990; Reizer et al., 1991). The ^1H and ^{15}N resonance assignments of the polypeptide backbone of the *B. subtilis* IIA^{Glc} domain (referred to hereafter as IIA^{Glc}) have been obtained by using three-dimensional ^1H–^{15}N heteronuclear NMR spectroscopy (Fairbrother et al., 1991). The structure of IIA^{Glc} has recently been determined independently by NMR spectroscopy (Fairbrother et al., 1992a) and X-ray crystallography (Liao et al., 1991). This paper reports an analysis of the backbone dynamics of the *B. subtilis* IIA^{Glc} domain from ^{15}N relaxation measurements performed by using inverse-detected ^1H–^{15}N 2D NMR techniques. The experimental ^{15}N relaxation data obtained have been analyzed using the model-free approach (Lipari & Szabo, 1982a).

Theory

The relaxation of protonated ^{15}N nuclei is mediated by the dipolar interactions with the directly attached protons and by chemical shift anisotropy (Abragam, 1961). The apparent longitudinal relaxation time constant, T_1, ignoring cross-correlation effects, is given by

$$1/T_1 = 1/T_1^{DD} + 1/T_1^{CSA} \quad (1)$$

in which T_1^{DD} and T_1^{CSA} are the dipolar and CSA longitudinal relaxation time constants, respectively. The apparent transverse relaxation time constant, T_2, ignoring cross-correlation effects, is given by

$$1/T_2 = 1/T_2^{DD} + 1/T_2^{CSA} + R_{ex} \quad (2)$$

in which T_2^{DD} and T_2^{CSA} are the dipolar and CSA transverse relaxation time constants, respectively, and R_{ex} is the sum of the effective rate constants for other pseudo-first-order processes that contribute to transverse relaxation, most notably ^{15}N conformational exchange (Bloom et al., 1965).

For a secondary amide ^{15}N nucleus, the dependencies of the dipolar relaxation rate constants on the spectral density function $J(\omega)$ are given by (Abragam, 1961; Lipari & Szabo, 1982a)

$$1/T_1^{DD} = (1/4)d_{NH}^2[J(\omega_H - \omega_N) + 3J(\omega_N) + 6J(\omega_H + \omega_N)] \quad (3)$$

$$1/T_2^{DD} = (1/8)d_{NH}^2[4J(0) + J(\omega_H - \omega_N) + 3J(\omega_N) + 6J(\omega_H) + 6J(\omega_H + \omega_N)] \quad (4)$$

in which

$$d_{NH} = (h/2\pi)(\mu_o/4\pi)\gamma_H\gamma_N\langle r_{NH}^{-3}\rangle \quad (5)$$

h is Plank's constant (6.626×10^{-34} J s), μ_o is the permeability of free space ($4\pi \times 10^{-7}$ T m A^{-1}), γ_H and γ_N are the gyromagnetic ratios of ^1H and ^{15}N (2.6752×10^8 and -2.7108×10^7 s^{-1} T^{-1}, respectively), ω_H and ω_N are the Larmor frequencies of ^1H and ^{15}N ($2\pi \times 500.13$ and $-2\pi \times 50.68$ MHz, respectively), and r_{NH} is the N–H bond length (0.102 nm). The spectral density function, $J(\omega)$, is the Fourier transform of the orientational correlation function of a unit vector along the N–H bond and incorporates the dependence of the relaxation rates on molecular motion. The CSA relaxation rate constants, assuming an axially symmetric chemical shift tensor, are

$$1/T_1^{CSA} = (1/3)\omega_N^2(\sigma_\parallel - \sigma_\perp)^2 J(\omega_N) \quad (6)$$

$$1/T_2^{CSA} = (1/18)\omega_N^2(\sigma_\parallel - \sigma_\perp)^2[4J(0) + 3J(\omega_N)] \quad (7)$$

in which $\sigma_\parallel$ and $\sigma_\perp$ are the parallel and perpendicular components of the chemical shift tensor ($\sigma_\parallel - \sigma_\perp = -160$ ppm; Hiyama et al., 1988). The steady-state NOE is

$$\text{NOE} = 1 + (1/4)T_1 d_{NH}^2(\gamma_H/\gamma_N)[6J(\omega_H + \omega_N) - J(\omega_H - \omega_N)] \quad (8)$$

Since there is generally insufficient experimental data to determine uniquely the spectral density functions in eq 3–8, the spectral density function is approximated by using an extended model-free formalism (Clore et al., 1990a; Lipari & Szabo, 1982a,b)

$$J(\omega) = (2/5)\left[\frac{S^2\tau_m}{1 + (\omega\tau_m)^2} + \frac{(S_f^2 - S^2)\tau}{1 + (\omega\tau)^2}\right] \quad (9)$$

in which $S^2 = S_f^2S_s^2$ is the generalized order parameter, which measures the degree of spatial restriction of the unit bond vector, S_f^2 is the order parameter for the rapid time scale motions, and S_s^2 is the order parameter for the slower time scale motions; $1/\tau = 1/\tau_m + 1/\tau_e$, τ_m is the overall rotational correlation time of the molecule, and τ_e is the effective internal correlation time describing internal motions on the slower of the two time scales; motions on the faster time scale are assumed to be very fast (<10 ps), and the overall tumbling of the molecule is assumed to be isotropic. If motions on two time scales are not resolvable, the original model-free formalism (Lipari & Szabo, 1982a,b) is recovered by defining $S_f^2 = 1$; consequently, τ_e becomes the effective correlation time for the detectable internal motions. The value of S^2 ranges from 0, generally taken to indicate isotropic internal motions (although specific anisotropic motional models can yield $S^2 = 0$; Lipari & Szabo, 1982a), to 1 for internal motion that is completely restricted, relative to a fixed molecular frame of reference. If all internal motions are very fast ($\tau_e \ll 10$ ps), the spectral density function (eq 9) is simplified to

$$J(\omega) = (2/5)S^2\tau_m/[1 + (\omega\tau_m)^2] \quad (10)$$

Experimental Procedures

Sample Preparation. The overproduction and purification of IIA^{Glc} have been described previously (Sutrina et al., 1990; Reizer et al., 1991). Uniform ^{15}N labeling (>95%) was performed by growing the cells in minimal medium containing $(^{15}NH_4)_2SO_4$ as the sole nitrogen source. NMR samples contained ~0.8 mM IIA^{Glc} in 10 mM potassium phosphate, pH 6.6 (90% H_2O/10% D_2O).

NMR Measurements. The pulse sequences used to record the ^1H-detected ^{15}N–^1H correlation spectra for measuring the ^{15}N T_1 and T_2 relaxation time constants and {^1H}–^{15}N NOEs

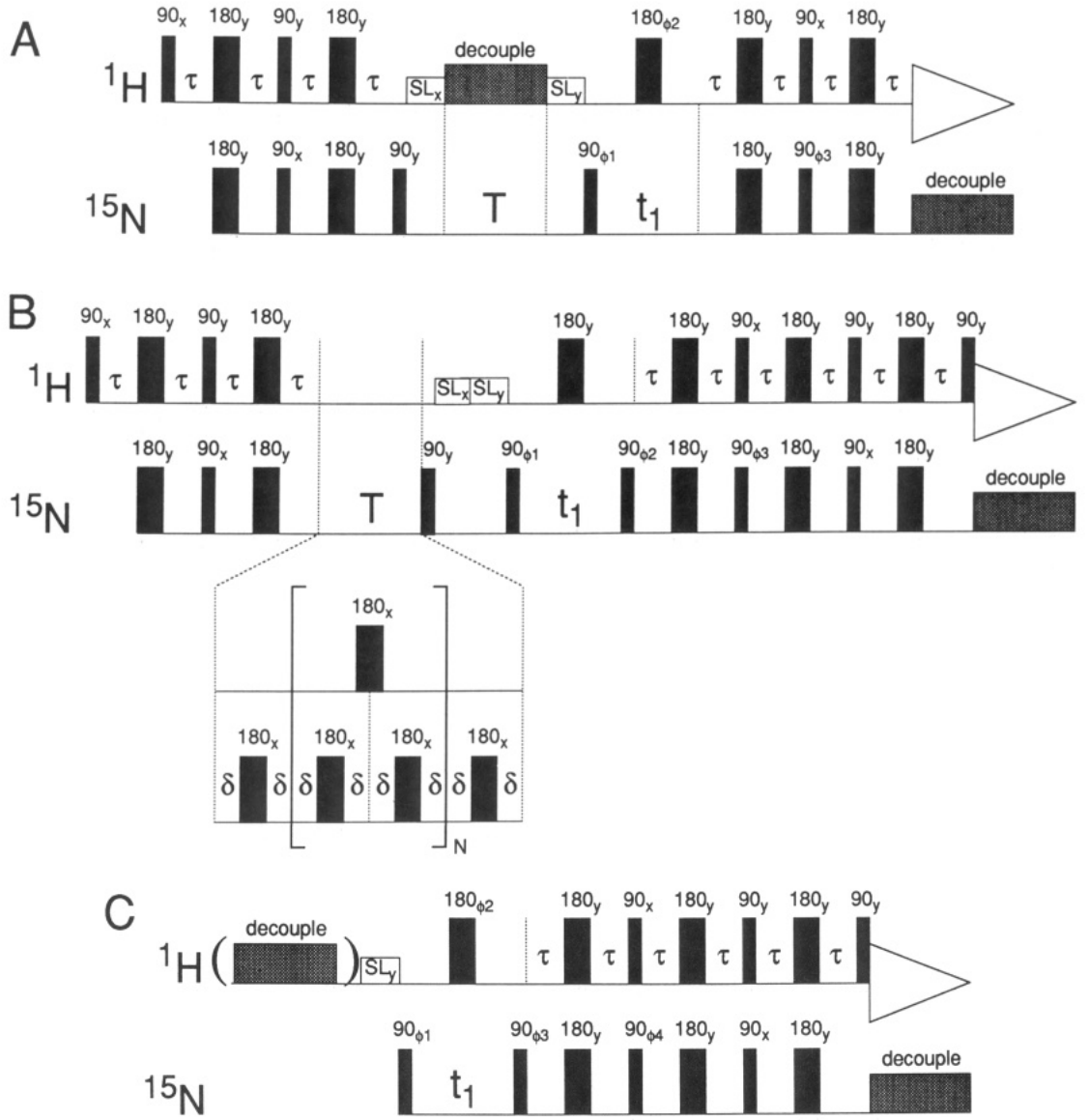

FIGURE 1: Pulse sequences used for measurement of ^{15}N (A) T_1 and (B) T_2 and (C) {^{1}H}–^{15}N NOE with ^{1}H detection. The phase cycling used for the T_1 experiment was $\phi 1 = 2(x, -x, x, -x, -x, x, -x, x)$, $\phi 2 = 16(y), 16(-y)$, $\phi 3 = 2(y, y, -y, -y), 2(-y, -y, y, y)$, and receiver = $x, -x, -x, x, 2(-x, x, x, -x), x, -x, -x, x$, with 32 transients being recorded per t_1 increment. Quadrature detection in ω_1 was achieved by applying time-proportional phase incrementation to $\phi 1$ (Marion & Wüthrich, 1983). The phase cycling used for the T_2 experiment was $\phi 1 = x, -x, x, -x, -x, x, -x, x$, $\phi 2 = y$ on odd FIDs and $-y$ on even FIDs, $\phi 3 = 2(y, y, -y, -y)$, and receiver = $x, -x, -x, x, -x, x, x, -x$, and 8 transients were recorded per FID; t_1 and $\phi 1$ were incremented every second FID. Odd and even FIDs were stored separately for later deconvolution to yield a spectrum equivalent to one acquired conventionally with 32 transients per t_1 increment (Palmer et al., 1991b). The phase cycling used for the {^{1}H}–^{15}N NOE experiment was $\phi 1 = 2(x, -x, x, -x, -x, x, -x, x)$, $\phi 2 = 16(y), 16(-y)$, $\phi 3 = y$ for odd FIDs and $-y$ for even FIDs, $\phi 4 = 2(y, y, -y, -y), 2(-y, -y, y, y)$, and receiver = $x, -x, -x, x, 2(-x, x, x, -x), x, -x, -x, x$. A total of 32 transients were recorded per FID, with t_1 and $\phi 1$ being increment every second FID. Odd and even FIDs were stored separately. The data were deconvoluted to yield two independent spectra, each equivalent to a conventionally acquired spectrum recorded with 64 transients per t_1 increment (Palmer et al., 1991b). Spin-lock purge pulses for water suppression are denoted SL. The value of τ was set to $1/(4J_{NH})$ ($\sim$2.75 ms).

are shown in Figure 1. The experiments used to measure the T_1 (Figure 1A) and T_2 (Figure 1B) time constants consisted of a refocused INEPT sequence (Morris & Freeman, 1979; Burum & Ernst, 1980) to transfer magnetization from the directly bound amide protons to the ^{15}N nuclei, a variable relaxation period, T, the t_1 evolution period, and a second refocused INEPT sequence to transfer magnetization from the ^{15}N back to the amide proton for detection. Proton decoupling, using GARP-1 (Shaka et al., 1985), was applied during the relaxation period of the T_1 experiment (Figure 1A) in order to eliminate the effects of dipolar cross-relaxation and cross-correlation between dipolar and anisotropic chemical shift relaxation mechanisms on the ^{15}N longitudinal relaxation (Boyd et al., 1990). A ^{15}N Carr–Purcell–Meiboom–Gill (CPMG) spin-echo sequence (Carr & Purcell, 1954; Meiboom & Gill, 1958) was applied during the transverse relaxation period, T, of the T_2 experiment (Figure 1B). The CPMG sequence minimizes the effects of resonance offset and field inhomogeneity and suppresses contributions from chemical exchange and scalar relaxation if $k\delta \ll 1$, where k is the exchange or scalar relaxation rate constant and δ is the CPMG spin-echo time (Bloom et al., 1965). The effects of cross-correlation upon the ^{15}N transverse relaxation were eliminated by application of ^{1}H 180° pulses synchronously with every second echo in the ^{15}N CPMG sequence (Palmer et al., 1992; Kay et al., 1992). The interval 2δ between the refocusing pulses in the ^{15}N CPMG sequence was $\sim$1.0 ms, which is sufficiently short to effectively spin-lock the heteronuclear spins (Vold & Vold, 1976; Palmer et al., 1992). The pulse scheme used for the measurement of the ^{15}N T_2 relaxation rate con-

stants employed the new sensitivity improvement method (Palmer et al., 1991b) in which two orthogonal in-phase proton magnetization components are detected, rather than the single component recorded in conventional experiments. This method allows spectra to be recorded with the same signal-to-noise ratio as the conventional method (after suitable deconvolution of the data) in approximately half the time. The same technique can be applied to the T_1 experiment but was not used in the present case. The experiment used to measure the $\{^1H\}$–^{15}N NOEs consisted of an initial relaxation delay (with or without ^1H saturation, corresponding to the presence or absence of the $\{^1H\}$–^{15}N NOE, respectively), the t_1 evolution period, and either a refocused INEPT sequence or a sensitivity-enhanced INEPT (shown in Figure 1C) to transfer magnetization to the amide proton for observation. GARP-1 was used for proton saturation during the relaxation delay. The 2D correlation spectra acquired with and without the $\{^1H\}$–^{15}N NOE were recorded in an interleaved manner in order to minimize differences in sample conditions. In the sensitivity-improved sequence, the two orthogonal in-phase components recorded were deconvoluted to produce two pure-phase spectra, each with a comparable signal-to-noise ratio to a conventional experiment recorded in the same time. The spectra thus obtained were not added to enhance the signal-to-noise ratios; instead, the NOE was calculated separately for each orthogonal component. In all experiments, ^{15}N was decoupled during acquisition using GARP-1.

All NMR spectra were recorded at 308 K on a Bruker AMX500 spectrometer, equipped with a three-channel interface. For the T_2 experiments, an auxiliary amplifier (Model 3205, American Microwave Technology) was required to generate high-power ^{15}N pulses at the repetition rate necessitated by the CPMG sequence. The duty cycle during the ^{15}N CPMG sequence was <10% in order to minimize contributions from sample heating and $T_{2\rho}$. A total of 4K complex points were acquired in ω_2, with a spectral width of 12.5 kHz and the ^1H carrier placed on the H_2O signal; 400 increments were collected in ω_1 with a spectral width of 1.75 kHz and the ^{15}N carrier at 116.4 ppm. Solvent suppression in all experiments was achieved by the use of spin-lock purge pulses (Messerle et al., 1989) and postacquisition application of a low-pass filter to the time domain data (Marion et al., 1989).

For measurements of T_1 and T_2 rate constants, a recycle delay of 1.9 s, which is approximately 3 times the ^1H T_1, was used between acquisitions to ensure sufficient recovery of ^1H magnetization. For measurements of the $\{^1H\}$–^{15}N NOE, a recycle delay of 4.1 s, approximately 5 times the longest ^{15}N T_1, was used between scans to ensure that maximal NOEs developed before acquisition. For T_1 measurements seven T delays of 44, 128, 247, 500, 1008, 2003, and 3000 ms were used, while for T_2 measurements eight T delays of 4, 42, 100, 200, 350, 500, 800, and 1200 ms were used. NOEs were measured twice by using the conventional sequence and twice by using a single sensitivity-enhanced experiment.

Data Analysis. Spectra were processed on a Sparc SLC computer using a modified version of the FTNMR software package (Hare Research). Each spectrum was processed twice in order to evaluate separately well-resolved and moderately overlapped cross-peaks. In the first instance, 6-Hz line broadening was applied in ω_2; in the second instance, a Lorentzian–Gaussian transformation was used. In both instances, a Lorentzian–Gaussian transformation followed by a cosine bell was used in ω_1. These weighting functions were selected to minimize the uncertainties in the measured peak heights while avoiding any systematic errors arising from cross-peak overlap or FID truncation artifacts. A simple spline baseline correction routine was employed in ω_2.

Relaxation rate constants and NOE enhancements were calculated from cross-peak heights in the ^1H–^{15}N correlation spectra. Data analysis was performed on a Convex C240 computer with programs written in FORTRAN 77; commercial (IMSL, Houston, TX) and published (Press et al., 1986) numerical algorithms were used as applicable. The uncertainties in the measured peak heights were estimated by repeating the experiments at several time points [T = 44 (twice), 247, 1008, and 3000 ms for T_1 measurements and T = 4, 100, 200, and 800 ms for T_2 measurements]. Differences between peak heights in the duplicate spectra were evaluated for a representative set of cross-peaks, and the standard deviation of the differences was divided by $\sqrt{2}$ to yield the uncertainty in the peak heights themselves (Palmer et al., 1991a). Uncertainties for those time points not duplicated were estimated by interpolation of the uncertainties for the duplicate pairs.

The longitudinal relaxation times, T_1, were obtained by a three-parameter nonlinear least squares fit of the equation

$$I(\mathrm{T}) = I_\infty - [I_\infty - I_0] \exp(-\mathrm{T}/T_1) \tag{11}$$

to the experimental data, while the transverse relaxation times, T_2, were obtained by two- or three-parameter nonlinear fits, respectively, of the equation

$$I(\mathrm{T}) = I_0 \exp(-\mathrm{T}/T_2) \tag{12}$$

or

$$I(\mathrm{T}) = I_\infty + I_0 \exp(-\mathrm{T}/T_2) \tag{13}$$

In eq 11–13, I_0 and I_∞ are the initial and final cross-peak heights, respectively. Curve fitting used the Levenburg–Marquardt algorithm (Press et al., 1986) to minimize the value of χ^2, given by

$$\chi^2 = \sum_{i=1}^{n} [I(\mathrm{T}_i) - \hat{I}(\mathrm{T}_i)]^2/\sigma_i^2 \tag{14}$$

in which $I(\mathrm{T}_i)$ is the experimental peak intensity, $\hat{I}(\mathrm{T}_i)$ is the intensity predicted from the values of the adjustable parameters in the model function at the ith time point, σ_i is the uncertainty in the ith experimental data point, and n is the number of time points recorded. Uncertainties in the relaxation rates were taken to be the standard errors of the fitted parameters.

The sufficiencies of the monoexponential decay functions given by eq 11–13 were evaluated with a χ^2 goodness-of-fit test, by comparing χ^2 (eq 14) to the 95% critical value of the χ^2 distribution, as described by Palmer et al. (1991a). For the T_2 data, the significance of the improvement afforded by the three-parameter model (eq 13) over the two-parameter model (eq 12) was evaluated using an F statistic (Ratkowsky, 1983; Wright et al., 1988) defined as

$$F = (n - 3)(\chi_2^2 - \chi_3^2)/\chi_3^2 \tag{15}$$

where χ_m^2 is the chi-squared goodness-of-fit statistic for the m-parameter model. The three-parameter fit was taken to be an improvement over the two-parameter fit only if the F statistic was greater than the 95% critical value of the distribution of F values. The critical value was determined from 500 Monte Carlo simulations (Palmer et al., 1991a) and was approximately equal to 5.12 (the tabulated value of $F_{9,1,0.05}$; Devore, 1982).

The steady-state NOEs were calculated as the ratios of peak heights in the spectrum recorded with proton saturation to those in the spectrum recorded without saturation; the average

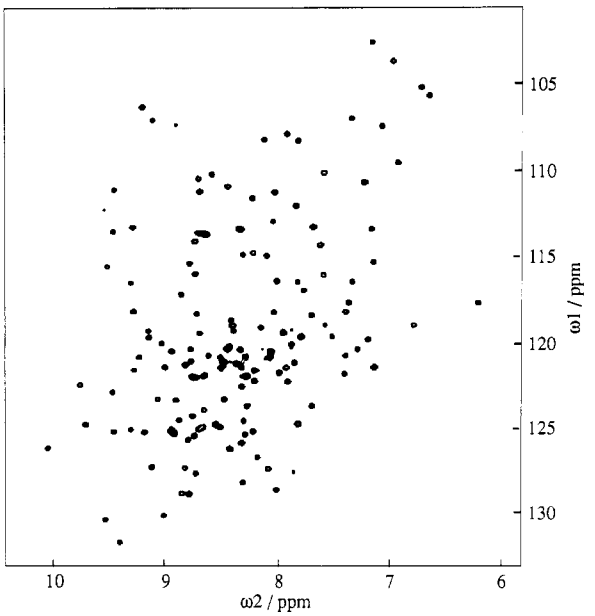

FIGURE 2: Negative level contour plot of the inversion–recovery experiment recorded with the pulse sequence shown in Figure 1A and a relaxation delay of T = 44 ms. The spectrum was processed to allow evaluation of the heights of the 113 well-resolved cross-peaks.

values of the NOEs and standard errors in the mean were determined from the four separate data sets.

Calculation of the model-free parameters from the measured relaxation rate constants and the NOE enhancements was performed by minimization of the target function

$$\chi^2 = \sum_{i=1}^{r} \Gamma_i = \sum_{i=1}^{r} [(R_{1i} - R_{1i}^*)^2/\sigma_{1i}^2 + (R_{2i} - R_{2i}^*)^2/\sigma_{2i}^2 + (\mathrm{NOE}_i - \mathrm{NOE}_i^*)^2/\sigma_{\mathrm{NOE}_i}^2] \quad (16)$$

in which Γ_i is the sum of the squared residuals; R_{1i}, R_{2i}, and NOE_i are the experimental values of the relaxation parameters; σ_{1i}, σ_{2i}, and σ_{NOE_i} are the uncertainties in the relaxation parameters; and R_{1i}^*, R_{2i}^*, and NOE_i^* are the values calculated with eq 1–8 for the ith amide ^{15}N nucleus. The summation extends over the r nuclei included in the calculation. As discussed below, model-free parameters were calculated using eq 9 or 10; an additional transverse relaxation term to account for ^{15}N conformational exchange on the time scale of the CPMG delay (R_{ex}, eq 2) was included in some analyses. Procedures used to find the optima of these parameters and to determine their uncertainties were identical to those described by Palmer et al. (1991a).

Results

Resolved Peaks. The ^{1}H and ^{15}N assignments of the backbone NH groups in IIA^{Glc} have been reported previously (Fairbrother et al., 1991, 1992b). In the present work, 113 cross-peaks were sufficiently well resolved in the correlation spectrum, processed with 6-Hz line broadening in ω_2, for peak heights to be measured accurately; an additional 24 peaks could be quantitated, albeit with slightly larger uncertainties, when a Lorentzian–Gaussian weighting function was applied in ω_2. Thus, T_1, T_2, and NOE data could be obtained for 137 (91%) of the 151 protonated backbone ^{15}N atoms.

As discussed elsewhere (Palmer et al., 1991a), more precise estimates of the relaxation rate constants and the NOE are obtained using peak heights rather than peak volumes to characterize the intensities of resonances in heteronuclear correlation spectra. Uncertainties in the peak heights for T_1

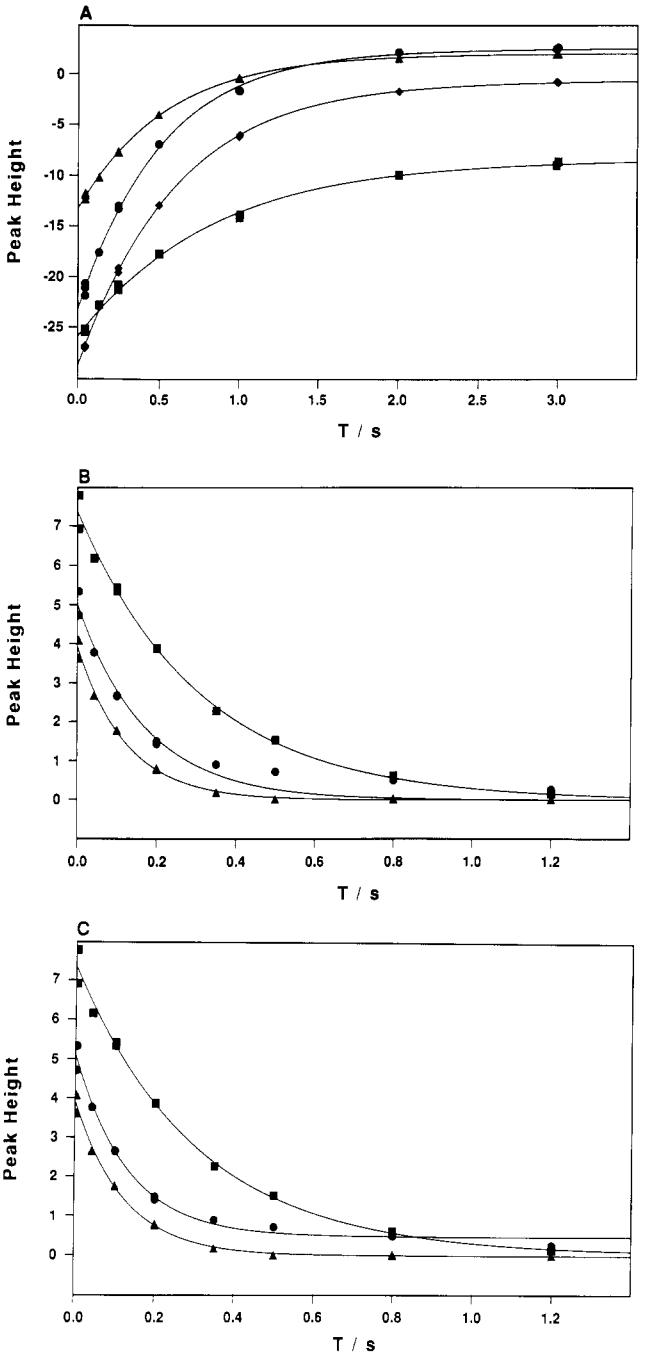

FIGURE 3: (A) T_1 relaxation curves, fit to eq 11, for S48 (▲), D116 (●), G11 (◆), and A3 (■). (B and C) T_2 relaxation curves, fit to eq 12 and 13, respectively, for L6 (■), V33 (●), and I86 (◆). Peak heights are shown on an arbitrary absolute scale; the uncertainties in the peak heights are less than 0.2 unit for T_1 curves and less than 1.2 units for T_2 curves. The data for L6 and I86 were fit better by eq 12, while the data for V33 were fit better by eq 13.

and T_2 measurements were estimated by recording several pairs of duplicate spectra. The variances in the peak heights were equal to the variances in the base-plane noise levels for the later time points of the CPMG experiment; however, for the earlier time points in this experiment and all the time points of the inversion–recovery experiment, the peak height uncertainties exceeded the rms noise levels by factors of 1.3–3.8. Both peak height uncertainties and rms noise levels decreased at later time points in the inversion–recovery and CPMG experiments; these effects may be correlated with improved suppression of the solvent signal at longer time points.

T_1 Values. The spectrum obtained from the first time point of the inversion–recovery experiment is presented in Figure

2. The peak heights of several resonances are plotted against time T in Figure 3A and fitted by nonlinear regression to a three-parameter exponential decay (eq 11). The decay constants, T_1, and uncertainties are plotted versus residue number in Figure 4A. For most residues, the T_1 values lie in the range 0.45–0.55 s. Although no T_1 values are lower than 0.45 s, several are conspicuously higher than 0.55 s. All residues from the N-terminus to E13 exhibit slow longitudinal relaxation, with the T_1 values decreasing roughly sequentially from 0.7–0.85 nearest the terminus to 0.56 at E13. Two other groups of residues, D31–F34 and A146–S149, have elevated longitudinal relaxation times, and the individual residues E22, D41, I51, F99, L136, G139, V142, and L162 also have larger than average T_1 values. The average uncertainties are 1.5% for well-resolved resonances (evaluated in the spectra processed with a line broadening function) and 2.5% for partially overlapped resonances (evaluated in the spectra processed with a Lorenztian–Gaussian transformation). In 72 out of 137 cases, the χ^2 test indicated that the fits were adequate statistically; in the remaining cases, the χ^2 values indicated that either the peak heights did not decay as single exponentials or the uncertainties in the peak heights had been somewhat underestimated. The fits did not statistically improve when double-exponential functions were used; consequently, the latter was assumed to be the case. Scaling the uncertainties to account for the observed χ^2 values would increase the average uncertainties to 2.2% and 3.8%, respectively (Palmer et al., 1991a).

T_2 Values. Curve fits were performed for two-parameter and three-parameter exponential functions (eq 12 and 13, respectively); examples of the fits are shown in panels B and C of Figure 3. T_2 relaxation data for 56 residues were fitted adequately by the two-parameter function, as adjudged by the χ^2 test. According to the F test, the fits for a further 66 residues did not improve when a third parameter was introduced. For the remaining 15 residues, the F parameter indicated that the three-parameter fit was an improvement over the two-parameter fit. A systematic difference, of unidentified origin, between the peak heights in the duplicate spectra of the first time point indicated that the uncertainties in the peak heights had probably been underestimated (as in the case of the T_1 measurements). Three-parameter fits were used for all residues for which the F parameter exceeded the 95% critical F value, while two-parameter fits were used for all other residues. The T_2 values and uncertainties are plotted in Figure 4B. Most residues have T_2 values in the range 0.11–0.15 s. None lie below this range, but as observed for the T_1 data, a number of residues exhibited slower relaxation; these included the N-terminal residues I2–E12, D31, Q32, D41, I51, L136, A146–S149, and L162. The average uncertainties are 1.6% and 2.6% for well-resolved and partially overlapped resonances, respectively. Scaling the uncertainties to account for the observed χ^2 values would increase the average uncertainties to 3.0% and 4.9%, respectively.

NOE Values. The NOE of each residue was determined for each data set as the ratio of the peak height in the spectrum recorded with proton saturation to that in the spectrum recorded without proton saturation. NOEs determined using conventional and sensitivity-enhancement methods were identical within experimental error. The average NOEs and uncertainties are plotted in Figure 4C. For most residues the NOEs are in the range 0.72–0.80, with only T88 and G93 having NOEs slightly above this range (0.83 and 0.81, respectively). The NOEs of residues I2–G11 and Q32 are negative, while the NOEs of E12–F15, D31, V33, I51, V142, A146–S149, D156, I157, and L162 are all less than 0.71. The average uncertainties are 1.3% for well-resolved resonances and 2.8% for partially overlapped resonances.

Effect of Amide Proton Exchange on the NOEs. If the T_1 of the water is sufficiently long and chemical exchange or spin diffusion between the amide protons and the water is sufficiently fast, the measured NOE may be artificially decreased as a result of incomplete equilibration of the amide ^{15}N and ^1H magnetization during the experiment acquired without proton saturation (Jelinski et al., 1980; Smith et al., 1987; Kay et al., 1989; Clore et al., 1990a). Kay et al. (1989) have chosen not to interpret NOEs in a quantitative manner; however, Clore et al. (1990a) and Kördel et al. (1992) have claimed that, in the cases of interleukin-1β and calbindin D_{9K}, respectively, these errors were sufficiently small to be ignored and have interpreted NOEs quantitatively within the framework of several different models for the spectral density function.

In the present work, the water T_1 was measured to be 4.5 s by using a 180–τ–90 pulse sequence and detuning the probe; the relevant relaxation delay was 4 s. Thus, if amide proton exchange approaches the intrinsic rate (ca. 10 s^{-1} at pH 6.6 and 35 °C; Englander & Poulsen, 1969; Molday et al., 1972; Wüthrich, 1986), the residual ^{15}N magnetization at the end of the relaxation period will be ca. 0.6 times its equilibrium intensity, and the measured NOE will be $NOE_0/(0.6 + 0.4NOE_0)$, in which NOE_0 is the actual NOE in the absence of amide proton exchange. In contrast, if the rate of proton exchange is much slower than ca. 0.25 s^{-1}, the measured NOE will be equal to NOE_0, while, for intermediate exchange rates, the amount by which the observed NOE differed from NOE_0 will depend on the exchange rate. Amide proton exchange rate constants for 71 of the 137 residues of IIA^{Glc} studied herein have been reported previously (Fairbrother et al., 1991). All of these residues have exchange rates much slower than required to cause errors in the NOEs. The remaining 66 residues have exchange rate constants greater than ca. 10^{-2} s^{-1}, the fastest rate able to be measured by the experiment used; thus, some of these residues may be in the exchange regime which would result in systematic errors in the NOEs. Indeed, amide proton exchange probably does contribute to the data for residue A3 because the measured NOE (-6.7 ± 0.7) is much lower than the theoretical minimum in the absence of exchange (−3.6). Using the above expression, an observed NOE of −6.7 would result from an NOE_0 of −1.1 for amide proton exchange at the intrinsic rate; more detailed calculations that explicitly include the rates of internal motions and amide proton exchange lead to similar conclusions (unpublished results). In order to ascertain whether exchange was affecting the NOEs for the 66 residues whose exchange rates had not been measured, model-free calculations were performed in which the NOEs were adjusted for presumed exchange effects (data not shown). These calculations indicated that exchange was not fast enough to affect the NOE for the majority of the residues. However, the most highly exposed residues, i.e., the N-terminal tail and possibly Q32, may be exceptions; therefore, dynamics parameters obtained for these residues should be interpreted only qualitatively. The dynamics parameters calculated using only T_1 and T_2 data show the same qualitative trends as those calculated using all three relaxation parameters, giving additional confidence in the accuracy of the NOE data (see supplementary material).

Initial Estimation of τ_m. Other workers (Kay et al., 1989; Clore et al., 1990a) have noted that, under conditions where $\tau_e < 100$ ps, $\tau_m > 1$ ns, and T_2 is not shortened significantly

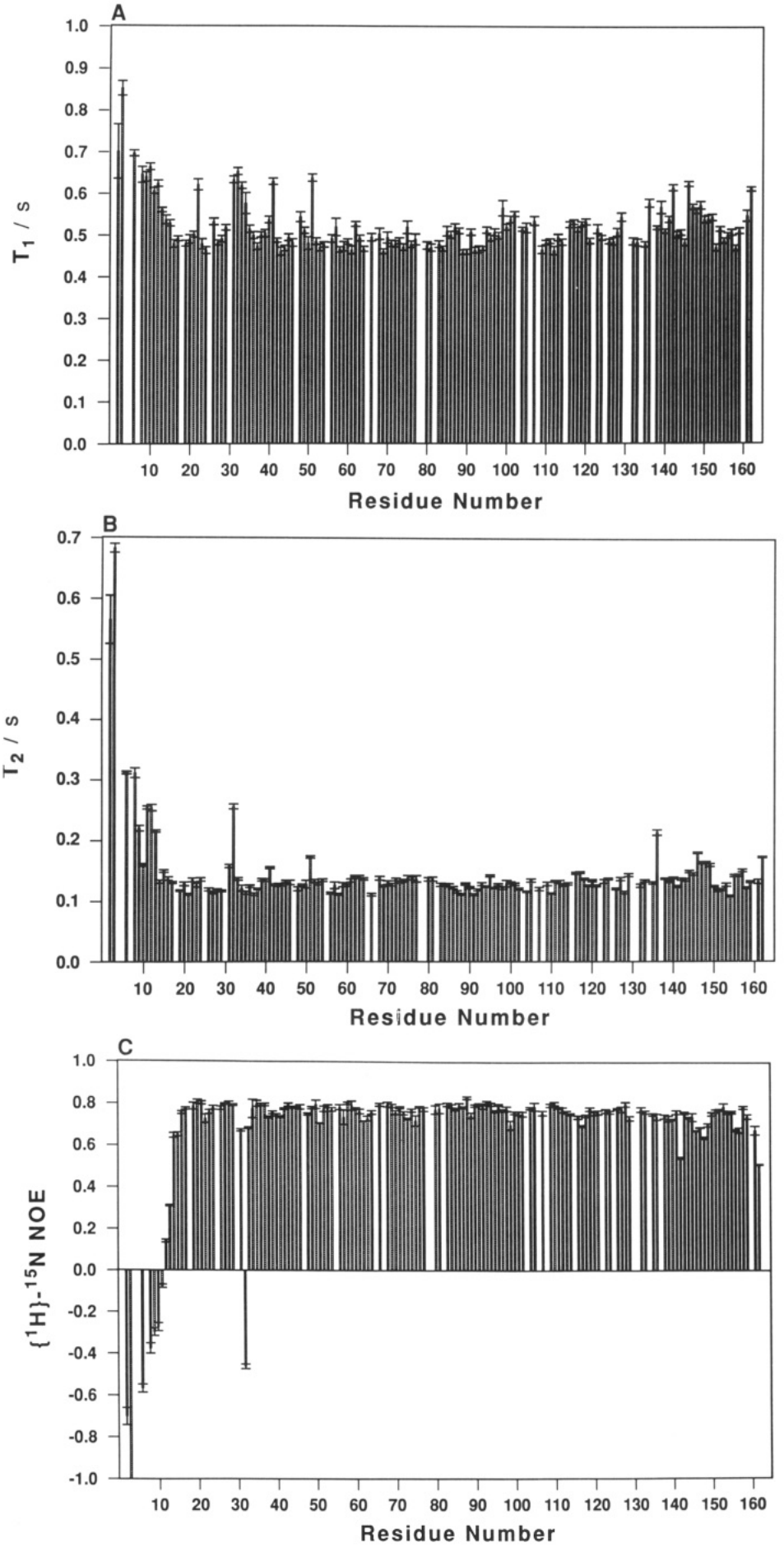

FIGURE 4: (A) T_1, (B) T_2, and (C) NOE values and uncertainties plotted for the 137 residues measured. T_1 and T_2 data were obtained by fitting the measured peak heights with eq 11–13, as appropriate. NOE values and their uncertainties are the averages and the standard errors, respectively, of the values determined from each of four data sets. The measured NOE of A3 (off scale) was -6.7 ± 0.7.

by chemical exchange, the ratio T_1/T_2 is essentially independent of S^2 and τ_e. The unusually high T_1 and T_2 values and low or negative NOE values noted above for the nine resolved resonances closest to the N-terminus and for Q32 clearly indicated that these residues were significantly more mobile than the rest of the molecule. Omitting the data for these 10 residues, the average T_1/T_2 ratio was used to estimate $\tau_m = 6.5 \pm 0.5$ ns, from eq 1-7 and 10. Subsequently, τ_m was optimized in the model-free analysis of the data for the remaining 127 residues. The τ_m value obtained from this calculation was fixed for the determination of the internal dynamics parameters for the 10 more mobile residues.

Selection of Optimization Parameters. As discussed earlier, several spectral density functions are possible, which vary in the degree of complexity of the internal motions. The simplest spectral density function (eq 10) is sufficient to account for the relaxation data only in cases when internal motions are extremely fast. Otherwise, τ_e must be included to account for internal motions (eq 9, $S_f^2 = 1$). Furthermore, if internal motions on two different time scales are resolvable, then separate order parameters can be included, each describing the degree of restriction of motions on a different time scale (eq 9, $S_f^2 < 1$). In addition, for certain resonances, a R_{ex} term (eq 2) must be included to allow for ^{15}N exchange broadening during the T_2 measurements. Omitting the data for residues 2-13 and Q32, the relaxation data for the remaining 127 residues were analyzed using the following selection criteria.

(a) Relaxation data for each residue were analyzed using the full single time scale spectral density function (eq 9, $S_f^2 = 1$) with τ_m fixed at 6.5 ns, the value estimated above. If the τ_e value obtained from this analysis was non-zero (within 95% confidence limits), then the data were analyzed using a spectral density function that included τ_e. Otherwise, a spectral density function excluding τ_e was used (eq 10).

(b) In a separate analysis, the relaxation data for each residue were fitted using the simplified spectral density function (eq 10), with τ_m fixed at 6.5 ns, but including an R_{ex} term to adjust for ^{15}N exchange broadening. As in (a), if R_{ex} was non-zero, then an adjustment for ^{15}N exchange broadening was made in the final analysis. Otherwise, no such adjustment was included in the calculation.

By applying these criteria, we selected 63 residues for analysis using the simplified spectral density function; for 20 of these, a ^{15}N exchange broadening term was included. The relaxation data for the remaining 64 residues were analyzed using the full spectral density function, with a R_{ex} term included for 20 of these residues. The internal dynamics parameters of all of these 127 residues and the τ_m value were then optimized simultaneously; i.e., 381 relaxation measurements were used to define 232 dynamics parameters. The optimized value of τ_m was 6.24 ± 0.01 ns. Following this analysis, the relaxation data for the 10 highly mobile residues were treated, with τ_m fixed at 6.24 ns, using the above criteria to select appropriate optimization parameters for each residue; τ_e was included in the analysis for all of these residues, while R_{ex} was included for all but two (A3 and L6). Thus, of the 137 residues studied, the relaxation data were analyzed by optimizing τ_e terms for 74 residues, R_{ex} terms for 48 residues, both τ_e and R_{ex} terms for 28 residues, and neither τ_e nor R_{ex} terms for 43 residues.

The order parameters, internal correlation times, and ^{15}N exchange terms are plotted in Figure 5. In most cases the order parameters are in the range 0.74-0.90. The N-terminal residues, I2-E13, are considerably less ordered ($S^2 < 0.55$), while other residues exhibiting order parameters lower than this range include V14, F15, E22, D31-F34, D41, I51, F99, E102, L117, G139, V142, A146-S149, and the C-terminal residue K162. The τ_e values are high (greater than ca. 50 ps) in the N-terminal region of the protein (I2-E13) and for Q32, while the only other residues with $\tau_e > 25$ ps are V14, F15, V142, G148, D156, I157, E161, and K162. Finally, the R_{ex} values indicate that in no case does conformational exchange cause the ^{15}N resonances to be broadened by more than 2 Hz. The model-free parameters and uncertainties in Figure 5 were calculated using the uncertainties in the relaxation times estimated by comparison of duplicate spectra. Scaling these uncertainties to account for the observed χ^2 values would not statistically change the model-free parameters but would cause the average uncertainty in the calculated order parameters to increase from 1.5% to 2.4%; this increase would not affect the conclusions reached about the dynamics of IIA^{Glc}.

Table I: Double Time Scale Dynamics Parameters[a]

residue	S_s^2	S_f^2	τ_e (ps)
I2	0.03 ± 0.04	0.73 ● 0.06	980 ± 47
L6	0.34 ± 0.01	0.75 ± 0.01	645 ± 18
N8	0.30 ± 0.02	0.77 ± 0.02	845 ± 42
G11	0.42 ± 0.01	0.77 ± 0.01	920 ± 25
E12	0.46 ± 0.02	0.71 ± 0.01	1131 ± 44
E13	0.53 ± 0.01	0.76 ± 0.01	1319 ± 34
Q32	0.43 ± 0.01	0.80 ± 0.01	523 ± 34

[a] Shown are the order parameters, S_s^2 and S_f^2, for slow and fast motions, respectively, and the internal correlation time, τ_e, for the slower of the two motional time scales, calculated using the double time scale spectral density function (eq 9). Data for a residue are included in the table if back-calculated relaxation parameters differed from the experimental data by more than 6% when only a single time scale was modeled, and the fits improved when a second time scale was introduced. The overall rotational correlation time was fixed at 6.24 ns for these calculations.

The sufficiencies of the fits in the above analyses were evaluated by comparing the experimentally determined relaxation data with relaxation parameters back-calculated from the optimized dynamics parameters. For 128 residues, the differences between these values were less than 6% for all three relaxation parameters. For A3, the difference of 59% between experimental and back-calculated NOEs was attributed to the effect of amide proton exchange, as discussed above. For the remaining eight residues, for which differences of greater than 6% occurred, model-free analyses were performed using the double time scale spectral density function (eq 9); τ_m was fixed at 6.24 ns and S_s^2, S_f^2, and τ_e were optimized. In the case of L136, this analysis did not yield realistic dynamics parameters. However, for the seven other residues, the relaxation data could be reproduced identically by the extended spectral density function; the results are listed in Table I.

Discussion

Pulse Sequences. The pulse sequences used in this work differ in several ways from those used by earlier workers to determine ^{15}N relaxation parameters (Kay et al., 1989; Clore et al., 1990a). First, effective water suppression was achieved simply by the application of spin-lock pulses rather than using DANTE or off-resonance DANTE pulse sequences. Second, in the previously reported sequences for longitudinal and transverse relaxation measurements, the t_1 evolution period preceded the relaxation period T, so the relaxation of only one of the two orthogonal magnetization components resulting from t_1 evolution could be observed. In the present sequences, the order of the t_1 and T periods has been reversed; this has allowed adaptation of the sequence for the measurement of transverse relaxation (Figure 1B) to detect both orthogonal

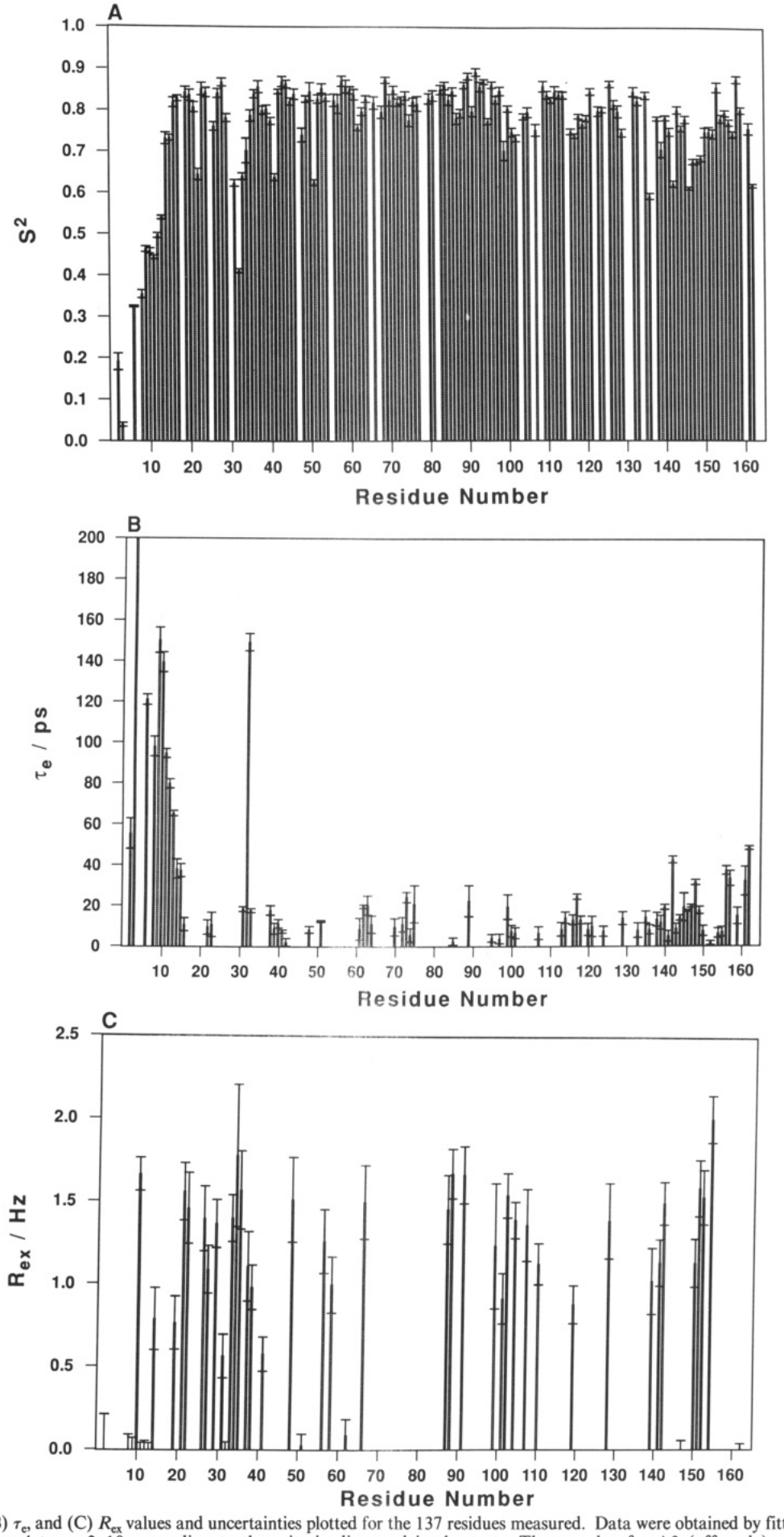

FIGURE 5: (A) S^2, (B) τ_e, and (C) R_{ex} values and uncertainties plotted for the 137 residues measured. Data were obtained by fitting the relaxation data shown in Figure 4 to eq 2–10, according to the criteria discussed in the text. The τ_e value for A3 (off scale) was 283 ± 14 ps.

magnetization components in a manner analogous to the previously developed "sensitivity-enhancement" sequences (Palmer et al., 1991b). [A similar modification can be employed for longitudinal relaxation measurements (Kördel et al., 1992).] Third, the transverse relaxation measurements (Figure 1B) have been performed using a modification of the CPMG technique in which proton 180° pulses are applied during the even CPMG echoes (Palmer et al., 1992). This method serves to eliminate contributions to the T_2 resulting from cross-correlation between dipolar and CSA relaxation mechanisms. Suppression of the effects of cross-relaxation and cross-correlation in the T_1 experiment was achieved by proton decoupling during the delay period T (Boyd et al., 1990). Finally, two independent determinations of the NOE were obtained for each single set of measurements made using the sensitivity-enhanced pulse sequences.

Model-Free Analyses. NMR studies of peptides in the solid state have indicated that the difference between parallel and perpendicular components of the ^{15}N chemical shift tensor is as much as 10 ppm smaller for peptides in a β-sheet conformation compared to those in an α-helical conformation (Shoji et al., 1989, 1990). Since no data exist to indicate whether this effect occurs for proteins in solution, the results reported herein were calculated using the value of −160 ppm that has been used elsewhere (Kay et al., 1989; Clore et al., 1990a,b); using a value of −150 ppm does not statistically change any of the calculated model-free parameters.

The models for the spectral density function used herein assume the overall rotational motion of the protein to be isotropic. The principal components of the inertial tensor of the globular part of IIA^{Glc} (residues 12–162) are calculated from the NMR structure (Fairbrother et al., 1992a) to be in the ratio 0.75:0.93:1.00. Therefore, the overall motions are not expected to be significantly anisotropic; this is consistent with the existence of a single rotational correlation time that adequately accounts for the experimental relaxation data.

Criteria are required to select the various model-free and exchange parameters that are necessary to satisfy the experimental data for each residue, because such selection generally cannot be made a priori on physical grounds. The deviation of the T_1/T_2 ratio for each residue from the mean ratio for all residues has commonly been used for variable selection (Clore et al., 1990a; Palmer et al., 1991a; Kördel et al., 1992). For example, Clore et al. (1990a) used the simplified spectral density function (eq 10) if the T_1/T_2 ratio was within one sample deviation of the mean, the Lipari–Szabo function (eq 9, $S_f^2 = 1$) if T_1/T_2 was more than one sample deviation below the mean, and the simplified spectral density function plus an exchange term if T_1/T_2 was more than one sample deviation greater than the mean. Once these selections had been made, an S_f^2 term was included to describe the restriction of internal motions on a very fast time scale (less than ca. 10 ps) if the NOE data could not be fitted satisfactorily. In the present instance, parameters have been selected for inclusion in the final model using Monte Carlo simulations of trial analyses that included the various possible terms. Application of the criteria of Clore et al. to the data for IIA^{Glc} leads to the inclusion of τ_e and R_{ex} terms for 10 and 21 residues, respectively. By contrast, using Monte Carlo simulations, 74 residues are selected to include τ_e, 48 to include R_{ex}, 28 to include both τ_e and R_{ex}, and only 43 to be analyzed by the simplified spectral density function without a ^{15}N exchange correction. In the optimization of the variables selected in this manner, the τ_e and R_{ex} terms for 5 and 11 residues, respectively, converged to zero, within 95% confidence limits (see supplementary material and Figure 5B,C). Thus, an extension of the Monte Carlo selection criteria is possible in which the terms for these residues are eliminated from a final analysis. All of the residues selected by the criteria of Clore et al. to include τ_e or R_{ex} are also selected by the simulations. However, our analyses revealed that a large number of additional residues had non-zero τ_e and/or R_{ex} values. In particular, high τ_e values were calculated for I10 ($\tau_e = 140 \pm 5$ ps), V14 ($\tau_e = 38 \pm 5$ ps), F15 ($\tau_e = 37 \pm 3$ ps), V142 ($\tau_e = 43 \pm 2$ ps), and L162 ($\tau_e = 48 \pm 1$ ps). Variable selection using the Monte Carlo simulations allows the data for a given residue to be analyzed using both τ_e and R_{ex} terms. These terms characterize motions that occur on widely differing time scales (picoseconds to nanoseconds as opposed to milliseconds) and are superimposed on each other. Cases in point include I10 ($\tau_e = 140 \pm 5$ ps, $R_{ex} = 1.7 \pm 0.1$ Hz) and V142 ($\tau_e = 43 \pm 2$ ps, $R_{ex} = 1.5 \pm 0.1$ Hz).

While the relaxation data for most residues were fitted adequately without inclusion of an order parameter describing the restriction of motions on an additional time scale, the fits for several residues in the more mobile region of the molecule improved markedly when a S_f^2 term was included (Table I). In the latter analyses, three dynamics parameters were fitted to three relaxation parameters for each residue; not surprisingly, values of the model-free parameters could be found that exactly reproduced the experimental data. However, for two residues in the mobile N-terminal region (E9 and I10), the fits did not improve when a S_f^2 term was included; since the N-terminal region is disordered, for the residues adjacent to E9 and I10 to exhibit mobility on two times scales, while E9 and I10 do not, is unlikely. Thus, without obtaining additional independent relaxation data for the N-terminal residues, the physical significance of the second time scale of motion indicated mathematically by these analyses cannot be assessed. Indeed, as already noted, the NOE data in this region may be affected by proton exchange; consequently, the dynamics data should be interpreted only qualitatively.

The extension of the spectral density function to model internal motions on two distinct time scales is formally equivalent to considering the overall motions of the molecule to be anisotropic (Lipari & Szabo, 1982a,b). In IIA^{Glc}, the residues that require such an extension are concentrated in the disordered N-terminal region, implying that anisotropic motions on a slow time scale may occur in this region of the molecule while the tumbling of the molecule as a whole remains isotropic. In this alternative conceptual description of the mathematical model, the parameters τ_m and τ_e (Table I) would be the respective correlation times for molecular tumbling and independent slow time-scale motions of the N-terminal region, S_s^2 would describe the relative contributions of these two types of motion to the correlation function, and S_f^2 would describe the degree of restriction of local internal motions, which are assumed to be very fast (less than ca. 10 ps).

Dynamics Parameters. The magnitudes of the dynamics parameters obtained in this study (Figure 5) are similar to those found in other studies of ^{15}N relaxation in proteins (Kay et al., 1989; Clore et al., 1990a; Kördel et al., 1992), with S^2 values typically in the range 0.75–0.95 and τ_e values generally less than ca. 50 ps. Clore et al. (1990a) have found that, for interleukin-1β, all residues exhibited fast motions on a time scale of ≤20–50 ps but that a number of residues also exhibited motions on a slower time scale (0.5–4 ns). In the present study, the residues listed in Table I may be classified as having both fast (≤20 ps) and slow (0.5–1.5 ns) internal motions. All other

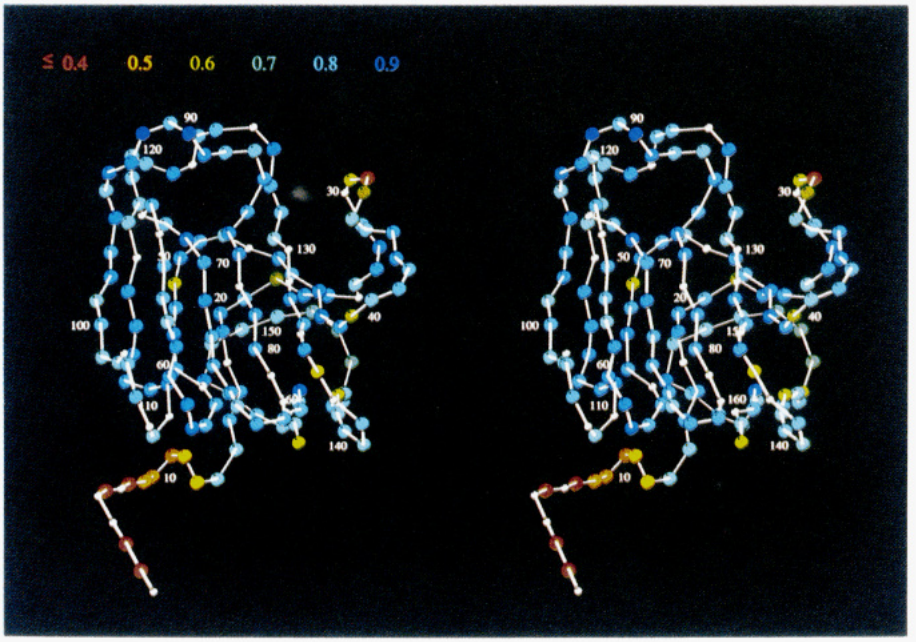

FIGURE 6: Schematic representation of the solution structure of *B. subtilis* IIA^{Glc} showing the amide nitrogen positions color-coded according to their calculated order parameters, S^2. Atoms are colored on a continuous scale from red ($S^2 \leq 0.4$) to indigo ($S^2 = 0.9$); backbone nitrogens for which order parameters were not calculated are shown as small white spheres. The coordinates used are the minimized averages from 15 distance geometry calculations of residues 12–162 (Fairbrother et al., 1992a); residues 1–11 were added in an extended conformation. Every tenth backbone nitrogen is labeled. This diagram was produced using the program MOLSCRIPT (Kraulis, 1991).

residues (with the exceptions of A3, E9, and I10, which are discussed above) exhibit only fast time-scale mobility (≤50 ps).

The calculated R_{ex} values (Figure 5C), which are indicative of motions on the millisecond time scale, do not show any correlation with either the τ_e values (Figure 5B) or the measured amide proton exchange rates (Fairbrother et al., 1991), which characterize motions on the picosecond to nanosecond and millisecond or longer time scales, respectively (Wagner, 1983). Thus, the physical significance of the ^{15}N exchange terms is difficult to establish in the absence of further experiments, such as $T_{1\rho}$ measurements, to characterize the absolute rates of the relevant motions.

The calculated dynamics parameters clearly indicate that there are several regions in IIA^{Glc} which are considerably more mobile than the rest of the molecule; the order parameters are represented mapped onto the protein structure in Figure 6. Most strikingly, the N-terminal residues, up to E13, are highly mobile, and the gradual increase in order parameters, from 0.2 at I2 to 0.73 at V14 and 0.82 at V16, suggests that the residues nearest to the terminus undergo essentially unrestricted motion while the N-terminal tail is anchored to the globular body of the protein loosely at residue 14 and more tightly at residue 16. This conclusion is in agreement with the observations from NOE correlation spectra, in which the residues up to E13 exhibit no medium- or long-range NOEs (Fairbrother et al., 1991). In the X-ray crystal structure of *B. subtilis* IIA^{Glc}, the N-terminal residues 4–13 have a unique conformation, although the crystallographic *B*-factors of residues 4–7 are high (Liao et al., 1991). The authors maintain that the conformation of the N-terminal region is not an artifact of crystallization; however, the solution state results discussed above suggest the contrary. That the N-terminal region is flexible in solution was anticipated because the first 13 residues have been defined as being part of the Q-linker which joins the IIA^{Glc} domain to the membrane-bound $IICB^{Glc}$ domain (Sutrina et al., 1990; Reizer et al., 1991). The order parameters at the C-terminus are also lower than for most residues, although in this case the more mobile region appears to consist of only two or three residues. This result is also consistent with the NOE data which indicate that the last three residues form an irregular β-structure.

The longest loop in IIA^{Glc} stretches from P25 to D41, between β-strands I and II [strand notation as in Fairbrother et al. (1991)]. This loop packs onto the β-sheet core of the protein with its apex close to the active site (Liao et al., 1991; Fairbrother et al., 1991, 1992a). The first six residues of this loop (P25–P30) as well as the residues from S35 to G40 exhibit normal order parameters. However, the residue at the C-terminal end of this loop, D41, and the four residues from D31 to F34 all have unusually low order parameters; residues D31 and F34 and the glycines on either side of D41 are totally conserved in members of the IIA^{Glc} protein family (Liao et al., 1991). Furthermore, D31, V33, M38, and G40 all have τ_e values in the range 10–20 ps, and seven residues in the region D31–D41 exhibit ^{15}N exchange broadening of 0.5 Hz or more. These data suggest that the region D31–D41 is considerably more mobile than the bulk of the molecule. The high mobility of this region and its proximity to the active site suggest that it may form part of the binding surface for HPr and/or enzyme IIB^{Glc}. Confirmation of this hypothesis must await structural and dynamical characterization of IIA^{Glc} that has been phosphorylated or is bound to another protein.

Another region of IIA^{Glc} that displays higher than normal mobility is the sequence from A146 to V150 (Figure 6). Residues 145–148 constitute a loop between two β-strands, and strand XII, from 149 to 152, forms a rather irregular β-structure with residues I19–E22 in the antiparallel strand I, as judged from the intensity of cross-strand NOEs (Fairbrother, unpublished results). Consistent with the high mobility of this region is the low order parameter (0.64) of E22, the residue directly opposite S149 in the β-structure.

Several other individual residues (I51, F99, E102, L117, G139, and V142) display low S^2 values. I51 is the first residue in a short β-strand (III). F99 forms part of a β-bulge at the C-terminal end of β-strand VII, while E102 is in the loop

immediately following the same β-strand. L117 is situated at the start of a long loop, which includes an irregular helix, between β-strands IX and X, while G139 is in a four-residue loop immediately preceding β-strand XI. The final mobile residue, V142, is situated directly opposite I160 in the two-stranded (XI and XIII) sheet; the hydrogen-bonding arrangement of this sheet may be continuously changing in response to the increased mobility of the three C-terminal residues.

In summary, while no obvious rules exist that allow predictions of which residues are likely to be particularly mobile, the observed mobilities can be rationalized in terms of the occurrence of disordered residues near termini, in loops or in regions of irregular structure. Of particular note, none of the residues in a regular β-structure have low order parameters.

ACKNOWLEDGMENTS

We thank Drs. Johan Kördel, Nicholas Skelton, and Walter Chazin for helpful discussions and for allowing us access to their data prior to publication. We also thank Dr. Mark Rance for useful discussions and technical assistance.

SUPPLEMENTARY MATERIAL AVAILABLE

One table giving the values and uncertainties, for each residue, of the experimentally determined T_1, T_2, and NOE data, the optimized order parameters, and (where applicable) internal correlation times and ^{15}N exchange broadening terms (dynamics parameters calculated by excluding the NOE data are also provided for the 10 highly mobile residues) (4 pages). Ordering information is given on any current masthead page.

REFERENCES

Abragam, A. (1961) *Principles of Nuclear Magnetism*, pp 264–353, Clarendon Press, Oxford.

Alger, J. R., & Shulman, R. G. (1984) *Q. Rev. Biophys. 17*, 83–124.

Bennett, W. S., & Huber, R. (1983) *CRC Crit. Rev. Biochem. 15*, 290–384.

Bloom, M., Reevers, L. W., & Wells, E. J. (1965) *J. Chem. Phys. 42*, 1615–1624.

Boyd, J., Hommel, U., & Campbell, I. D. (1990) *Chem. Phys. Lett. 175*, 477–482.

Burum, D. P., & Ernst, R. R. (1980) *J. Magn. Reson. 39*, 163–168.

Carr, H. Y., & Purcell, E. M. (1954) *Phys. Rev. 94*, 630–638.

Clore, G. M., Driscoll, P. C., Wingfield, P. T., & Gronenborn, A. M. (1990a) *Biochemistry 29*, 7387–7401.

Clore, G. M., Szabo, A., Bax, A., Kay, L. E., Driscoll, P. C., & Gronenborn, A. M. (1990b) *J. Am. Chem. Soc. 112*, 4989–4991.

Dean, D. A., Reizer, J., Nikaido, H., & Saier, M. H., Jr. (1990) *J. Biol. Chem. 265*, 21005–21010.

de Boer, M., Broekhuizen, C. P., & Postma, P. W. (1986) *J. Bacteriol. 167*, 393–395.

Devore, J. L. (1982) *Probability and Statistics for Engineering and the Sciences*, Brooks/Cole, Monterey.

Englander, S. W., & Poulsen, A. (1969) *Biopolymers 7*, 379–393.

Englander, S. W., & Kallenbach, N. R. (1983) *Q. Rev. Biophys. 16*, 521–655.

Fairbrother, W. J., Cavanagh, J., Dyson, H. J., Palmer, A. G., III, Sutrina, S. L., Reizer, J., Saier, M. H., Jr., & Wright, P. E. (1991) *Biochemistry 30*, 6896–6907.

Fairbrother, W. J., Gippert, G. P., Reizer, J., Saier, M. H., Jr., & Wright, P. E. (1992a) *FEBS Lett. 296*, 148–152.

Fairbrother, W. J., Palmer, A. G., III, Rance, M., Reizer, J., Saier, M. H., Jr., & Wright, P. E. (1992b) *Biochemistry 31*, 4413–4425.

Fedotov, V. D., & Kivayeva, L. S. (1987) *J. Biomol. Struct. Dyn. 4*, 599–619.

Gurd, F. R. N., & Rothgeb, T. M. (1979) *Adv. Protein Chem. 33*, 73–165.

Hiyama, Y., Niu, C.-H., Silverton, J. V., Bavoso, A., & Torchia, D. A. (1988) *J. Am. Chem. Soc. 110*, 2378–2383.

Jelinski, L. W., Sullivan, C. E., & Torchia, D. A. (1980) *J. Magn. Reson. 41*, 133–139.

Karplus, M., & McCammon, J. A. (1983) *Annu. Rev. Biochem. 53*, 263–300.

Kay, L. E., Torchia, D. A., & Bax, A. (1989) *Biochemistry 28*, 8972–8979.

Kay, L. E., Nicholson, L. K., Delaglio, F., Bax, A., & Torchia, D. A. (1992) *J. Magn. Reson.* (in press).

Kraulis, P. J. (1991) *J. Appl. Crystallogr. 24*, 945–949.

Led, J. J., Gesmar, H., & Abildgaard, F. (1989) *Methods Enzymol. 176*, 311–329.

Liao, D.-I., Kapadia, G., Reddy, P., Saier, M. H., Jr., Reizer, J., & Herzberg, O. (1991) *Biochemistry 30*, 9583–9594.

Lipari, G., & Szabo, A. (1982a) *J. Am. Chem. Soc. 104*, 4546–4559.

Lipari, G., & Szabo, A. (1982b) *J. Am. Chem. Soc. 104*, 4559–4570.

London, R. E. (1980) in *Magnetic Resonance in Biology* (Cohen, J. S., Ed.) pp 1–69, Wiley, New York.

Magasanik, B. (1970) in *The Lactose Operon* (Beckwith, J. R., & Zieser, D., Eds.) pp 189–219, Cold Spring Harbor Laboratory, Cold Spring Harbor, NY.

Marion, D., & Wüthrich, K. (1983) *Biochem. Biophys. Res. Commun. 113*, 967–974.

Marion, D., Ikura, M., & Bax, A. (1989) *J. Magn. Reson. 84*, 425–430.

Meadow, N. D., Fox, D. K., & Roseman, S. (1990) *Annu. Rev. Biochem. 59*, 497–542.

Meiboom, S., & Gill, D. (1958) *Rev. Sci. Instrum. 29*, 688–691.

Messerle, B. A., Wider, G., Otting, G., Weber, C., & Wüthrich, K. (1989) *J. Magn. Reson. 85*, 608–613.

Molday, R. S., Englander, S. W., & Kallen, R. G. (1972) *Biochemistry 11*, 150–158.

Morris, G. A., & Freeman, R. (1979) *J. Am. Chem. Soc. 101*, 760–762.

Nageswara Rao, B. D. (1989) *Methods Enzymol. 176*, 279–311.

Nelson, S. O., Wright, J. K., & Postma, P. W. (1983) *EMBO J. 2*, 715–720.

Nirmala, N. R., & Wagner, G. (1988) *J. Am. Chem. Soc. 110*, 7557–7558.

Nirmala, N. R., & Wagner, G. (1989) *J. Magn. Reson. 82*, 659–661.

Novotny, M. J., Frederickson, W. L., Waygood, E. B., & Saier, M. H., Jr. (1985) *J. Bacteriol. 162*, 810–816.

Osumi, T., & Saier, M. H., Jr. (1982) *Proc. Natl. Acad. Sci. U.S.A. 79*, 1457–1461.

Palmer, A. G., III, Rance, M., & Wright, P. E. (1991a) *J. Am. Chem. Soc. 113*, 4371–4380.

Palmer, A. G., III, Cavanagh, J., Wright, P. E., & Rance, M. (1991b) *J. Magn. Reson. 93*, 151–170.

Palmer, A. G., III, Skelton, N. J., Chazin, W. J., Wright, P. E., & Rance, M. (1992) *Mol. Phys. 75*, 699–711.

Postma, P. W., Epstein, W., Schuitema, A. R. J., & Nelson, S. O. (1984) *J. Bacteriol. 158*, 351–353.

Press, W. H., Flannery, B. P., Teukolsky, & Vetterling, W. T. (1986) *Numerical Recipes*, Cambridge University Press, Cambridge.
Ratkowsky, D. (1983) *Nonlinear Regression Modeling*, Marcel Dekker, New York.
Reizer, J., Saier, M. H., Jr., Deutscher, J., Grenier, F., Thompson, J., & Hengstenberg, W. (1988) *CRC Crit. Rev. Microbiol. 15*, 297-338.
Reizer, J., Sutrina, S. L., Wu, L.-F., Deutscher, J., & Saier, M. H., Jr. (1991) *J. Biol. Chem.* (in press).
Ringe, D., & Petsko, G. (1985) *Prog. Biophys. Mol. Biol. 45*, 197-235.
Roder, H. (1989) *Methods Enzymol. 176*, 446-473.
Saier, M. H., Jr. (1989) *Microbiol. Rev. 53*, 109-120.
Saier, M. H., Jr., Novotny, M. J., Comeau-Fuhrman, D., Osumi, T., & Desai, J. D. (1983) *J. Bacteriol. 155*, 1351-1357.
Shaka, A. J., Barker, P. B., & Freeman, R. (1985) *J. Magn. Reson. 64*, 547-552.
Shoji, A., Ozaki, T., Fujito, T., Deguchi, K., Ando, S., & Ando, I. (1989) *Macromolecules 22*, 2860-2863.
Shoji, A., Ozaki, T., Fujito, T., Deguchi, K., Ando, S., & Ando, I. (1990) *J. Am. Chem. Soc. 112*, 4693-4697.
Smith, G. P., Yu, L. P., & Domingues, D. J. (1987) *Biochemistry 26*, 2202-2207.
Sutrina, S. L., Reddy, P., Saier, M. H., Jr., & Reizer, J. (1990) *J. Biol. Chem. 265*, 18581-18589.
Vold, R. R., & Vold, R. L. (1976) *J. Chem. Phys. 64*, 320-332.
Wagner, G. (1983) *Q. Rev. Biophys. 16*, 1-57.
Welch, G. R., Somogyi, B., & Damjanovich, S. (1982) *Prog. Biophys. Mol. Biol. 39*, 109-146.
Williams, R. J. P. (1979) *Biol. Rev. 54*, 389-437.
Williams, R. J. P. (1989) *Eur. J. Biochem. 183*, 479-497.
Wootton, J. C., & Drummond, M. H. (1989) *Protein Eng. 2*, 535-543.
Wright, L. L., Palmer, A. G., III, & Thompson, N. L. (1988) *Biophys. J. 54*, 463-470.
Wüthrich, K. (1986) *NMR of Proteins and Nucleic Acids*, p 24, Wiley, New York.
Zang, L., Laughlin, M. R., Rothman, D. L., & Schulman, R. G. (1990) *Biochemistry 29*, 6815-6820.

Two-Dimensional NMR Studies of d(GGTTAATGCGGT)·d(ACCGCATTAACC) Complexed with the Minor Groove Binding Drug SN-6999†

Shiow-meei Chen, Werner Leupin,‡ Mark Rance, and Walter J. Chazin*
Department of Molecular Biology, The Scripps Research Institute, 10666 North Torrey Pines Road, La Jolla, California 92037
Received October 11, 1991; Revised Manuscript Received March 6, 1992

ABSTRACT: The dodecadeoxynucleotide duplex d(GGTTAATGCGGT)·d(ACCGCATTAACC) and its 1:1 complex with the minor groove binding drug SN-6999 have been prepared and studied by two-dimensional ^{1}H nuclear magnetic resonance spectroscopy. Complete sequence-specific assignments have been obtained for the free duplex by standard methods. The line widths of the resonances in the complex are greater than those observed for the free duplex, which complicates the assignment process. Extensive use of two-quantum spectroscopy was required to determine the scalar correlations for identifying all of the base proton and most of the 1′H–2′H–2″H spin subsystems for the complex. This permitted unambiguous sequence-specific resonance assignments for the complex, which provides the necessary background for a detailed comparison of the structure of the duplex, with and without bound drug. A series of intermolecular NOEs between drug and DNA were identified, providing sufficient structural constraints to position the drug in the minor groove of the duplex. However, the combination of NOEs observed can only be rationalized by a model wherein the drug binds in the minor groove of the DNA in both orientations relative to the long helix axis and exchanges rapidly between the two orientations. The drug binds primarily in the segment of five consecutive dA–dT base pairs d($T_3T_4A_5A_6T_7$)·d($A_{18}T_{19}T_{20}A_{21}A_{22}$), but surprisingly strong interactions are found to extend one residue in the 3′ direction along each strand to G_8 and C_{23}. The observation of intermolecular contacts to residues neighboring the AT-rich region demonstrates that the stabilization of the bis(quaternary ammonium) heterocycle family of AT-specific, minor groove binding drugs is not based exclusively on interactions with dA–dT base pairs.

The therapeutic activity of one of the primary classes of antitumor drugs is known to occur by interference with DNA metabolism via reversible binding in one of the grooves of double-stranded DNA helices (Zimmer & Wähnert, 1986; Lambert & LePecq, 1987). One family of this class of antitumor agents is characterized by binding in the minor groove of duplex DNA and includes the well-known oligopeptide antibiotics distamycin and netropsin as well as the bis(quaternary ammonium) heterocycles (bQAHs).[1] This family of

† This work was supported in part by grants from the National Science Foundation (DMB 8903777 to M.R.) and from the American Cancer Society (JFRA-294 and CH-529 to W.J.C.).
‡ Present address: Pharma Division, Preclinical Research, F. Hoffmann La Roche, Ltd., Basel, Switzerland.

[1] Abbreviations: bQAH, bis(quarternary ammonium) heterocycle; CD, circular dichroism; UV, ultraviolet; NMR, nuclear magnetic resonance; 1D, one dimensional; 2D, two dimensional; COSY, correlated spectroscopy; 2Q, two-quantum spectroscopy; TOCSY, total correlation spectroscopy; NOE, nuclear Overhauser effect; NOESY, 2D NOE spectroscopy; EDTA, ethylenediaminetetraacetic acid; d_i(A;B), intranucleotide distance between protons A and B; d_s(A;B), sequential distance between protons A and B, where A is in the 5′ direction relative to B.

0006-2960/92/0431-4406$03.00/0